frontiers in Materials

ORIGINAL RESEARCH
published: 12 January 2022
doi: 10.3389/fmats.2021.787729

# High-Temperature Tribological Behavior of $Al_{0.3}Cr_{0.5}Fe_{1.5}Mn_{0.5}Ni$ High-Entropy Alloys With Addition of Titanium and Carbon

*Chun-Hao Peng*[1,2], *Che-Wei Tsai*[1,2]*, *Chia-Ming Kuo*[1,2] *and Sheng-Min Chiu*[1,2]

[1]Department of Materials Science and Engineering, National Tsing Hua University, Hsinchu, Taiwan, [2]High Entropy Materials Center, National Tsing Hua University, Hsinchu, Taiwan

In this study, the $Al_{0.3}Cr_{0.5}Fe_{1.5}Mn_{0.5}Ni$ high-entropy alloys (HEAs) with addition of titanium and carbon was prepared. The as-cast alloys were composed of FCC solid solution and TiC particles, and were further aged and strengthened by precipitation of B2-NiAl phase at 700°C for 10 h to increase hardness from Hv 200 to Hv 400. Tribological properties of the HEAs and commercial tool steel (AISI M2) against $Al_2O_3$ under dry sliding condition at room-temperature and elevated temperatures are compared. After high-temperature wear testing, the HEAs demonstrated exceptional oxidation resistance and a lower friction coefficient than M2 steel since the dense glazed layer on the surface of the HEAs served as a lubricant to decrease the friction coefficient, and protected the substrate from oxidation.

**Keywords: high-entropy alloys, high-temperature tribology, titanium carbide, glazed layer, metal matrix composite**

OPEN ACCESS

***Edited by:***
*E-Wen Huang,*
*National Yang Ming Chiao Tung University, Taiwan*

***Reviewed by:***
*Shuangxi Song,*
*Shanghai Jiao Tong University, China*
*Yuting Lv,*
*Shandong University of Science and Technology, China*

***Correspondence:**
*Che-Wei Tsai*
*chewei@mx.nthu.edu.tw*

***Specialty section:***
*This article was submitted to Mechanics of Materials, a section of the journal Frontiers in Materials*

***Received:*** *01 October 2021*
***Accepted:*** *04 November 2021*
***Published:*** *12 January 2022*

***Citation:***
*Peng C-H, Tsai C-W, Kuo C-M and Chiu S-M (2022) High-Temperature Tribological Behavior of $Al_{0.3}Cr_{0.5}Fe_{1.5}Mn_{0.5}Ni$ High-Entropy Alloys With Addition of Titanium and Carbon. Front. Mater. 8:787729. doi: 10.3389/fmats.2021.787729*

## INTRODUCTION

In recent years, the demand for industrial machinery in extreme environments has been increasing. High-temperature tribological behavior is one of the major life-limiting factors for tool steels (Inman et al., 2003; Jiang et al., 2005; Pauschitz et al., 2008). The significant role of high temperature sliding wear was first identified by Fink, (1930). Oxidation resistance is particularly concerned with high-temperature wear since an oxide layer might form on the surface and help to decrease the friction coefficient (Stott, 1998; Aoh and Chen, 2001). Moreover, the dense oxide layer known as "glazed layer" is formed during wear and decreases the wear rate and friction coefficient. The better oxidation resistance exhibited by alloys leads to the formation of a denser oxide layer, the lubrication mechanism such as self-lubrication were also shown in several alloys (Pei et al., 2005; Deng et al., 2007). Several studies have been conducted on the tribological performance of traditional alloys at elevated temperatures (Birol, 2010; Inman and Datta, 2011; Cheng et al., 2017; Khajuria and Wani, 2017); the mechanism of glazed layer has also been well-researched (Stott et al., 1973; Stott, 1998; Jiang et al., 2004). The main objective of the present work is to investigate the tribological behavior of high-entropy alloys (HEAs) at elevated temperatures.

HEAs have been suggested to contain at least five principal metal elements, each of which constitutes more than 5 at% but less than 35 at% (Yeh et al., 2004). HEAs exhibit exceptional mechanical properties, such as increased hardness, elongation, and satisfactory thermal stability (Chen et al., 2010; Tsai et al., 2010; Hsu et al., 2011; Juan et al., 2015). The distinctive features of HEAs are attributable to four core effects (Yeh, 2015; Miracle and Senkov, 2017): high-entropy effect, which enhances the formation of single solid solution phase, such as face-centered cubic (FCC) or body-centered cubic (BCC) phase; severe lattice distortion, which results from the atomic size difference among different elements in the solid solution phase and affects the mechanical properties; sluggish diffusion, which is due to the inefficient cooperative diffusion of

**TABLE 1 |** The nominal compositions of the HEAs in this study (at%).

| | Al | Cr | Fe | Mn | Ni | Ti | C |
|---|---|---|---|---|---|---|---|
| $Al_{0.3}Cr_{0.5}Fe_{1.5}Mn_{0.5}NiTi_{0.2}C_{0.2}$ (TC02) | 7.1 | 11.9 | 35.7 | 11.9 | 23.8 | 4.8 | 4.8 |
| $Al_{0.3}Cr_{0.5}Fe_{1.5}Mn_{0.5}NiTi_{0.5}C_{0.5}$ (TC05) | 6.3 | 10.4 | 31.3 | 10.4 | 20.8 | 10.4 | 10.4 |

various species that slows down the phase transformation (however, further research is required to confirm this); cocktail effect, which results from the interactions among the components in solid solution.

Previous studies regarding the $Al_{0.3}CrFe_{1.5}MnNi_{0.5}$ alloys (Chen et al., 2010; Tsao et al., 2012; Chuang et al., 2013; Tsai et al., 2013) demonstrated that they exhibit a significant age-hardening phenomenon with hardness increasing from Hv 400 to Hv 900. Tsai et al. confirmed that the hardening effect results from the formation of the σ phase (Tsai et al., 2013). Chen et al. demonstrated that other phases such as Cr-rich BCC, B2-NiAl compound existed in the alloys (Chen et al., 2010). Additionally, other strengthening methods of HEAs are also conducted. Studies regarding $(FeCrNiCo)Al_xCu_y$ alloys (Fan et al., 2014) demonstrated that it was reinforced by the uniformly distributed TiC ceramic particles and the hardness increased from Hv 400 to Hv 600 with the addition of TiC. The mechanical properties of HEAs such as strength, elongation, and hardness have been well-researched. However, studies concerned with the high-temperature tribological properties are limited (Alvi and Akhtar, 2019; Chen et al., 2019; Du et al., 2019; Joseph et al., 2019; Liu et al., 2019; Prabhu et al., 2019).

Based on these research findings, the matrix of the as-prepared alloy was designed according to the $Al_{0.3}CrFe_{1.5}MnNi_{0.5}$ HEA. The component of the matrix was modified into $Al_{0.3}Cr_{0.5}Fe_{1.5}Mn_{0.5}Ni$, which changes the structure from BCC to FCC; besides, TiC particles were formed by adding titanium and carbon during melting to increase the strength and tribological performance. In this study, the microstructure and mechanical properties of the HEAs after heat treatment were investigated. Moreover, wear testing against counterpart $Al_2O_3$ under the dry sliding condition at room-temperature and elevated temperatures was conducted and the results were compared with those of AISI M2 high-speed steel, which is widely used in high-temperature applications.

## MATERIALS AND METHODS

The bulk alloys with the molar ratio of $Al_{0.3}Cr_{0.5}Fe_{1.5}Mn_{0.5}NiTi_{0.2}C_{0.2}$ and $Al_{0.3}Cr_{0.5}Fe_{1.5}Mn_{0.5}NiTi_{0.5}C_{0.5}$ (designated TC02 and TC05) were produced by arc-melting elemental Al, Cr, Fe, Mn, Ni, Ti, and C with purity exceeding 99.95 wt% under an argon atmosphere at least four times to ensure compositional homogeneity. The dimension of the solidified ingots was about 50 × 10 × 10 mm. The nominal bulk compositions are shown in **Table 1**.

To elucidate the aging and precipitation behavior, the ingots were aged at 700°C for 10 h. Microstructural analysis was conducted using a combination of X-ray diffraction (XRD), scanning electron microscopy (SEM), and energy-dispersive X-ray spectroscopy (EDS). Scanning electron images and backscattered electron images were obtained using a JEOL IT100 SEM, equipped with an Oxford x-act energy-dispersive X-ray spectroscopy. XRD data were collected on a Bruker D2 PHASER XRD instrument with Cu-Kα radiation at 30 kV and 20 mA. Scans were conducted at a rate of 0.14 deg/s. The hardness profile was determined using a Vickers hardness tester (Matsuzawa Seiki MV-1) with a load of 5 kg and a duration of 12 s.

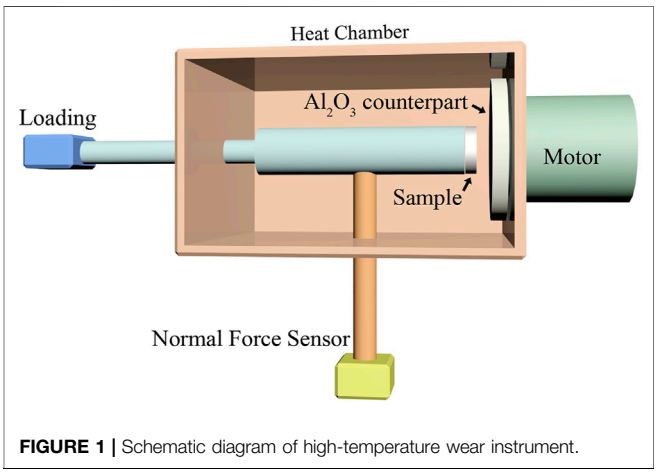


**FIGURE 1 |** Schematic diagram of high-temperature wear instrument.

High-temperature tribological properties of the as-prepared alloys were evaluated using a pin-on-disc type tester under dry sliding conditions, as shown in **Figure 1**. The wear specimen was locked on the holder connected to the horizontal and vertical force load cell, which detected the friction and normal force respectively, and the normal force was driven by pneumatic cylinder to ensure the stable normal force. The dimension of the specimen was φ8 × 3 mm, and each of the specimen was grinded to #4000 with SiC paper. Wear tests were conducted at room temperature and 700°C with a sliding speed of 0.5 m/s, under 3 kg load for 100 min. During the test, the specimen was held on the counterpart material at diameter of 50 mm, and the motor would whirl the counterpart material at 377 rpm, which equals to relative linear speed of 0.5 m/s for the specimen. The tests were repeated three times to ensure confidence in results. To ensure the specimens can be worn under elevated temperature, the counterpart material is composed of $Al_2O_3$ with the diameter of 75 mm, the thickness of 10 mm, the hardness of Hv 1,600, the average roughness (Ra) of 5 μm, and the relative density of 0.997. Tribological quantification was conducted via measuring the worn area and the cross-sectional microstructure was analyzed using SEM, XRD, and EDS.

## RESULTS AND DISCUSSION

### Analysis of Microstructure and Hardness

The composition of the matrix was designed based on the statistics of the related parameters such as valence electron

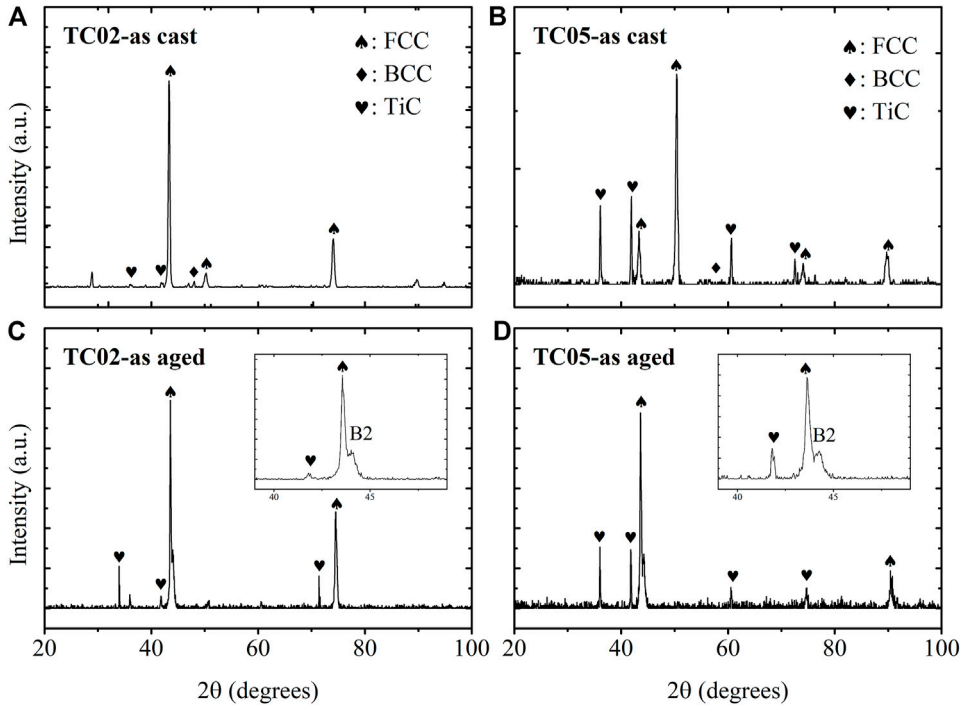


**FIGURE 2 |** XRD of **(A)** as-cast TC02, **(B)** as-cast TC05, **(C)** as-aged TC02, and **(D)** as-aged TC05 alloys.

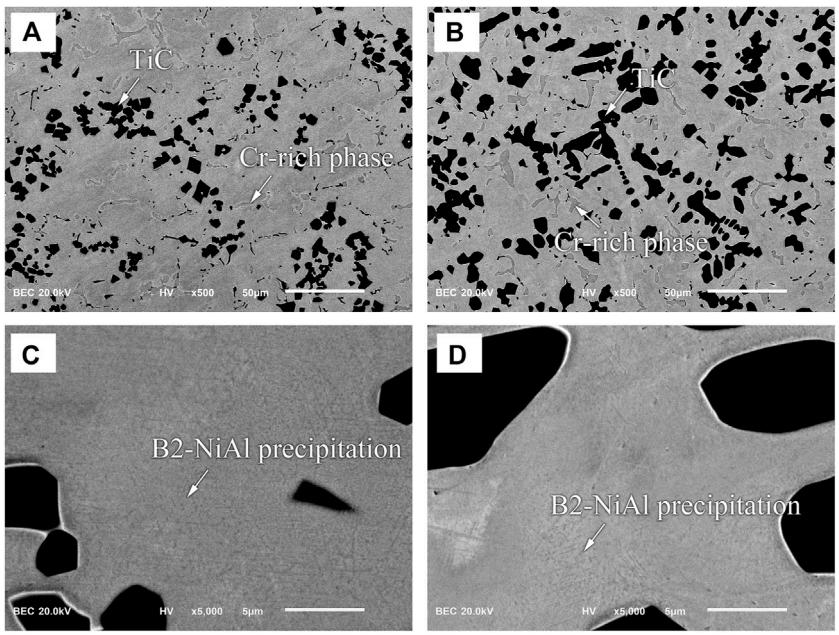


**FIGURE 3 |** SEM of **(A)** as-cast TC02, **(B)** as-cast TC05, **(C)** as-aged TC02, and **(D)** as-aged TC05 alloys.

concentration (VEC), δ, and Ω (the ratio of mixing entropy and mixing enthalpy) to predict the phase simulation since TiC would not dissolve in the matrix. The matrix composition of both HEAs was the same besides the difference in TiC addition. The VEC, δ, and Ω values of the matrix were 7.74, 3.6%, and 2.83, respectively. According to the statistical results of Guo's research (Guo et al., 2011), FCC phases were observed to be stable at higher VEC (≥8), and that of the as-prepared matrix was 7.74. In addition, Ω ≥ 1.1

**TABLE 2 |** EDS analysis of as-cast alloys (at%).

| | | Al | Cr | Fe | Mn | Ni | Ti | C |
|---|---|---|---|---|---|---|---|---|
| As-cast TC02 | Matrix | 8.0 | 13.6 | 41.5 | 10.9 | 25.5 | 0.4 | - |
| | Cr-rich | 5.0 | **36.9** | 29.0 | 10.5 | 18.6 | 0.5 | - |
| | TiC | 0.4 | 0.9 | 0.8 | 0.4 | 0.4 | **65.9** | **31.2** |
| As-cast TC05 | Matrix | 8.2 | 12.6 | 41.6 | 7.0 | 28.9 | 2.1 | - |
| | Cr-rich | 3.9 | **47.6** | 25.1 | 11 | 11.9 | 0.7 | **-** |
| | TiC | 0.4 | 1.8 | 1.9 | 0.5 | 0.9 | **47.7** | **46.8** |

**TABLE 4 |** Mixing enthalpy of principle elements (kJ/mol) (Takeuchi and Inoue, 2005).

| | Al | Cr | Fe | Mn | Ni |
|---|---|---|---|---|---|
| Al | – | −10 | −11 | −19 | −22 |
| Cr | – | – | −1 | 2 | 4 |
| Fe | – | – | – | −2 | −2 |
| Mn | – | – | – | – | −8 |
| Ni | – | – | – | – | – |

**TABLE 3 |** Hardness and vol% of TiC of both alloys.

| | Hardness ($Hv_5$) (as-cast) | Hardness ($Hv_5$ (as-aged) | Vol% of TiC (theoretical) | Vol% of TiC (experimental) |
|---|---|---|---|---|
| TC02 | 238.6 | 368.7 | 6.9 | 8.5 |
| TC05 | 312.4 | 498.8 | 17.7 | 18.4 |

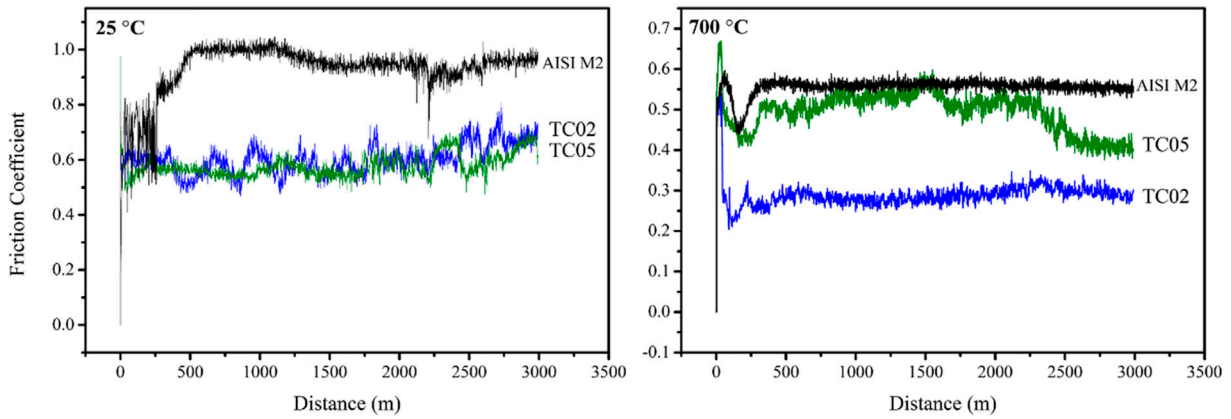


**FIGURE 4 |** Friction coefficient curves of as-prepared alloys.

and $\delta \leq 6.6\%$ were proposed as a criterion for forming a solid-solution phase based on the prediction of Yang et al. (Yang and Zhang, 2012). The as-prepared matrix could be expected to be a solid-solution phase composed of a major FCC phase and a minor BCC phase, depending on the VEC, δ, and Ω values.

Furthermore, aging treatment was conducted for the HEAs at 700°C for 10 h to enhance the mechanical strength. **Figure 2** shows the XRD patterns of as-cast and as-aged alloys. Both as-cast alloys were composed of a major FCC phase and a minor TiC phase. The SEM images of the HEAs are shown in **Figure 3**. It can be observed that both TC02 and TC05 possessed a light gray matrix, a separated gray eutectic phase, and separated black particles at the as-cast state. Their chemical compositions are listed in **Table 2**. Further, the result is compared with the XRD analysis, which shows that the matrix was FCC; the gray phase was Cr-rich BCC, and the black particles tended to be TiC, while the proportion of BCC phase was too small to be detected by XRD. The Cr-rich BCC phase might form during the cooling process of arc-melting, which was also observed in the $Al_xCrFe_{1.5}MnNi_{0.5}$ alloys (Chen et al., 2010). The size of TiC particles in TC02 and TC05 was approximately 10 μm, while certain TiC particles with smaller size were also formed in the matrix. Moreover, the volume ratio of TiC in the TC05 alloy was higher than that in TC02 due to the higher content of Ti and C elements in the alloy. The volume fraction of TiC and hardness of both as-cast and as-aged HEAs are summarized in **Table 3**.

The XRD patterns of the as-aged alloys are shown in **Figure 2**. The BCC peaks, which correspond to the age-hardening phase, appeared after the aging treatment. The microstructure of both alloys after the aging treatment was similar to their as-cast state (**Figure 3**), where the matrix was FCC; the gray phase was Cr-rich BCC, and the black particles tended to be TiC, while the black stripe-like precipitates were formed in the matrix of the peak-aged alloys. These precipitates were primarily of the B2-NiAl compound since Ni-Al possesses the highest mixing enthalpy among all elements in the matrix (**Table 4**); this indicates a tendency to form a Ni-Al compound in the matrix. This could also correspond to the BCC peaks in the XRD patterns and the increase in hardness. This phenomenon was also reported in a

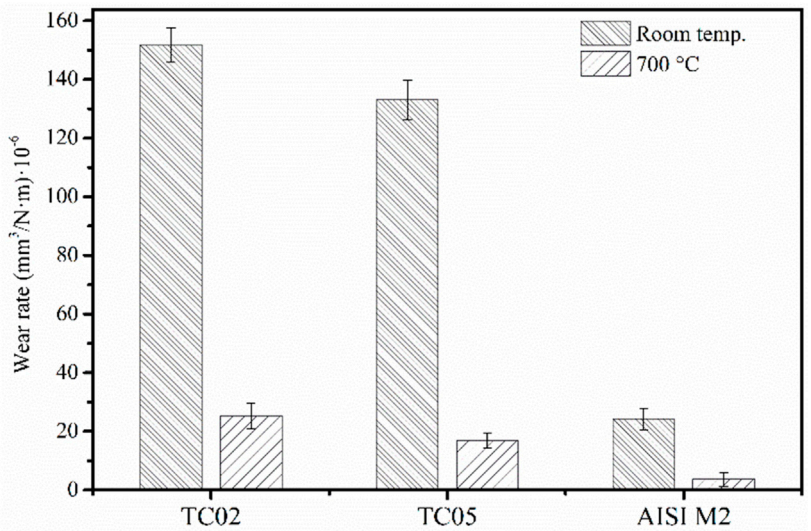


**FIGURE 5 |** Wear rate of the alloys at 25°C and 700°C.

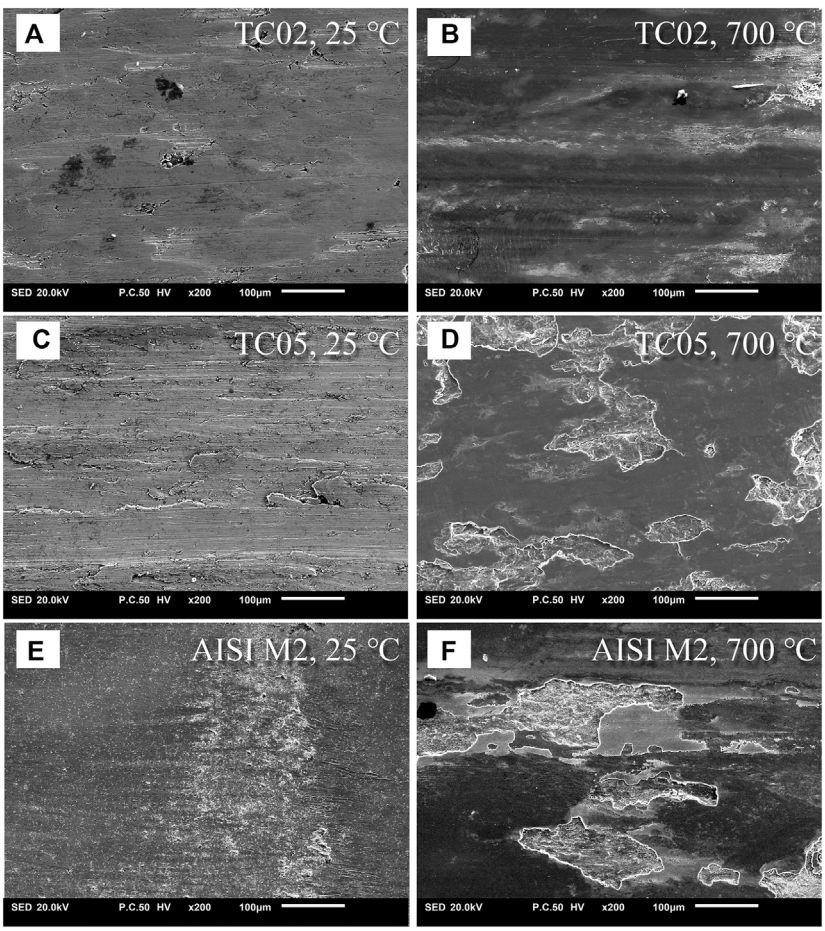


**FIGURE 6 |** SEI images of the worn surface of **(A,C,E)** alloys at room temperature and **(B,D,F)** at 700°C.

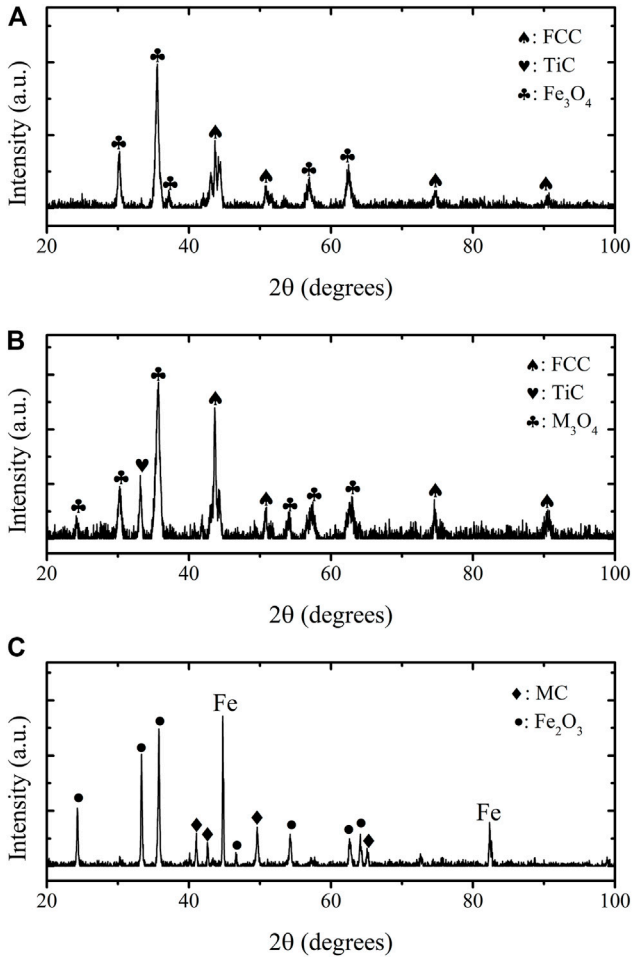


**FIGURE 7 |** XRD patterns of **(A)** TC02 alloy, **(B)** TC05 alloy, and **(C)** M2 steel after wear testing at 700°C.

previous study (Chen et al., 2010). The TC02 and TC05 alloys exhibited the same precipitation phenomenon due to the same composition of the matrix. The size and distribution of the TiC particles would not change because the melting point of TiC is higher than the aging temperature, and the C element has the most negative mixing enthalpy with the Ti element than any other component. The width of the B2 precipitates was approximately 10 nm, and the length was approximately a few micrometers. Such nanoscaled precipitates harden the alloys and increase the hardness. Wear testing was further conducted for both the as-aged alloys to measure the tribological properties.

## Tribological Properties at Ambient and Elevated Temperature

**Figure 4** shows the friction coefficient curves of the TC02, TC05 as-aged alloys, and M2 steel against $Al_2O_3$ counterpart during pin-on-disc wear testing at 25°C and 700°C. Since the results of the repeated tests are similar, only one result is displayed to facilitate comparison in **Figure 4**. Both TC02 and TC05 alloys had a lower friction coefficient of approximately 0.60, while M2 steel had the higher friction coefficient of approximately 0.90° at 25°C. At 700°C, TC02 alloy possessed the lowest friction coefficient of approximately 0.29 among the three alloys. TC05 alloy had a medium friction coefficient of approximately 0.5, while M2 steel had a highest friction coefficient of approximately 0.56. This shows that both the HEAs exhibit a lower friction coefficient than commercial M2 steel. **Figure 5** shows the wear rate of the alloys. The wear rate of M2 steel was lower than that of both HEAs at room and elevated temperature. It is noticeable that the wear rate of the HEAs decreased dramatically at an elevated temperature. The SEM analysis of the worn surface is shown in **Figure 6**. All the HEAs and M2 steel at 700°C possessed a glazed layer on the worn surface. The glazed layer formed on the surface served as a lubricant resulting in a low friction coefficient (**Figure 4**). There was no glaze layer on the worn surface of M2 after room-temperature wear, which results in the highest friction coefficient among all results. On the other hand, there were shallow and fewer grooves on the worn surface of M2 steel compared with both HEAs after room-temperature wear testing, which a possessed lower wear rate at room-temperature (**Figure 5**). After high-temperature testing, there were fewer depletion regions on the worn surface of the TC02 alloy and several depletion regions on that of the TC05 alloy and M2 steel, which possessed the higher friction coefficient (**Figure 4**). **Figure 7** shows the XRD analysis of the tested samples. Only the XRD results of the sample after high-temperature wear testing are displayed since the glaze layer of the alloys after room-temperature wear testing was too thin to be detected by the XRD instrument. Both the HEAs after wear testing showed the peaks of $Fe_3O_4$, while M2 steel showed the peaks of $Fe_2O_3$. This indicates that the difference in the friction coefficient is mainly due to the distribution of the glazed layer.

## Discussion of Tribological Behavior

According to the result of the surface analysis, the cross-sectional microstructure was further observed using SEM and EDS line scanning (**Figures 8**, **9**) to clarify the difference in the glaze layer properties of each alloy. There was only the mixing layer which is a mixture of substrate and oxide formed on the surface of both HEAs after room-temperature wear test in **Figures 8A,D**. The dense glaze layer was formed after elevated temperature wear test in **Figures 8B,E**. Since the mixing layer was not composed of a dense oxide, it would be formed and split frequently, resulting in the higher and unstable friction coefficient and wear rate at room temperature. The dense glaze layer served as a better lubricant to decrease the friction coefficient and wear rate, which results in a lower friction coefficient and wear rate at elevated temperatures (**Figures 4**, **5**).

**Figures 8B,C** show that there were three layers under the surface of the TC02 alloy. Based on the EDS analysis, the first layer was a thin (3 μm) and dense glazed layer composed of

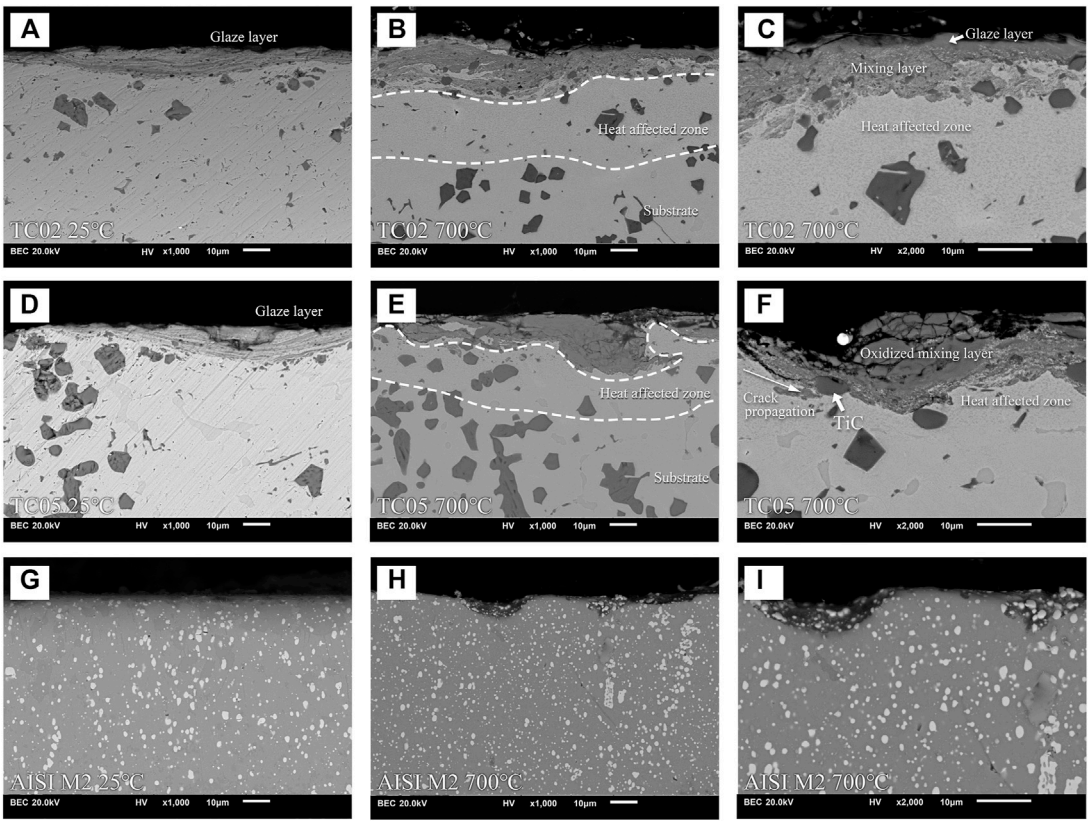


**FIGURE 8 |** Cross-sectional microstructure of the worn surface under 25 and 700°C: **(A–C)** are TC02 alloy; **(D–F)** are TC05 alloy; **(G–I)** are M2 steel.

iron oxide, which corresponds to $Fe_3O_4$ analyzed via XRD. The second layer was a mixture of oxide and substrate, and the oxygen content was observed to gradually decrease with the increasing depth. The mixing layer was approximately 9 μm in thickness. The final layer was the heat-affected zone, B2-NiAl precipitates were coarsened since the substrate near the surface was heated by friction. According to these layers as mentioned above, the substrate and counterpart material were in contact and wore directly and formed a mixing layer during the initial wear process, which is also observed on the surface of the HEAs after room-temperature wear testing and corresponds to the higher amplitude of the friction coefficient. As time increased, the oxidized debris was deposited on the surface and transformed into a glazed layer under high temperature and pressure, and then protected the substrate from further wear; thus, the friction coefficient was reduced (**Figure 4**).

Similar layers were observed near the surface of the TC05 alloy, as shown in **Figure 8E** and the formation mechanism was the same: The mixing layer was formed during the initial wear process, and the glazed layer was formed subsequently on the surface to protect the substrate. However, the distribution of the mixing layer was different. The glazed layer of the TC05 alloy was hemispherical and did not distribute satisfactorily because of a significant amount of TiC. This shows that oxygen invaded the substrate; according to **Figure 8F** oxygen propagates in alignment with the interface of TiC and the matrix, and the crack also propagates in alignment with the arrow to TiC. The thickness of the mixing layer could be up to 20 μm. Finally, the mixing layer was oxidized and decreased the interface strength of the substrate and mixing layer. Owing to this phenomenon, the oxide layer was split easily and was unable to partially protect the substrate and then increase the friction (**Figure 4**).

Unlike the distribution of the oxide layer on the surface of TC02 and TC05 alloys, neither the glazed layer nor mixing layer was observed near the surface of M2 steel. Moreover, the related signal was not observed during the EDS analysis (**Figure 9**). Nevertheless, a thick oxide layer could be observed on the other side of the sample (i.e., non-worn surface) of M2 steel (**Figure 10**), while few oxide layers were observed on that of both HEAs. This indicates that either the oxidation resistance of M2 steel was too weak to form the dense glazed layer during high-temperature wear testing, or the oxide layer had been split easily during grinding or polishing. When the wear testing was conducted on M2 steel, the oxide layer was formed on the surface at first; then the oxide layer split owing to its excessive thickness, and then the oxide layer split owing to its excessive

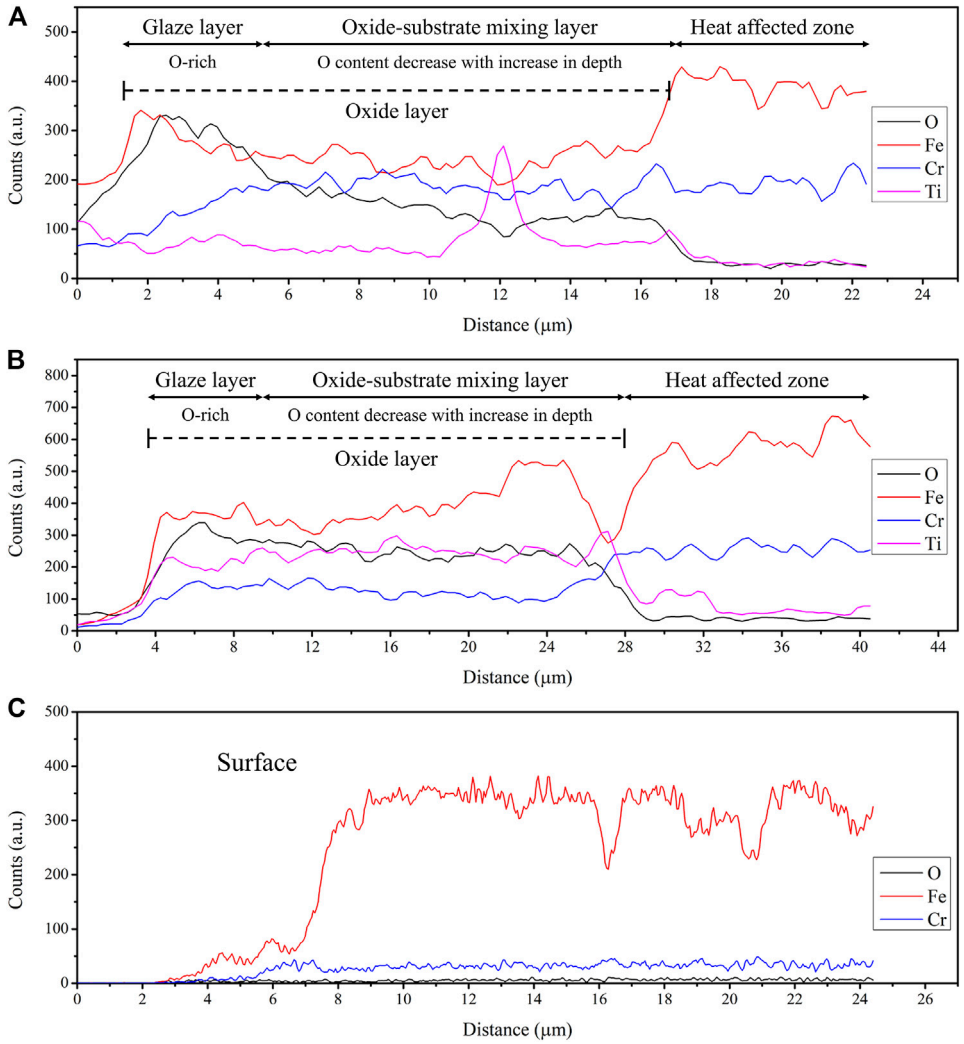


**FIGURE 9 |** EDS line scan of **(A)** TC02 alloy, **(B)** TC05 alloy, and **(C)** M2 steel (Only partial elements which changed significantly were selected to simplify the figure).

thickness, exposing a new substrate to oxidation; this process is repeated several times. The repeated oxidation and surface roughness increased the friction coefficient (**Figure 4**). In addition, the wear rate of high-temperature wear is affected by the weight gain of oxidation and the weight loss of wear. During high-temperature wear testing, only one surface of the alloys was worn while all the surfaces were oxidized simultaneously. It reveals that better oxidation resistance of the HEAs led to less weight gain by oxidation, and poor oxidation resistance of the M2 steel caused more weight gain, which might actually possess a higher wear rate than experimental results.

Both HEAs exhibited fairly exceptional oxidation resistance compared to the poor oxidation resistance of M2 steel. The HEAs formed a dense glazed layer to protect the substrate and decreased the friction coefficient at elevated temperatures. This shows that the exceptional oxidation resistance of HEAs has the potential to be utilized in high-temperature applications. Furthermore, the TC02 alloy has the appropriate TiC content and continuous dense glazed layer, which indicates a significant high-temperature tribological performance.

## CONCLUSION

The as-prepared HEAs were composed of an FCC matrix, Cr-rich BCC interdendrite, and scattered TiC particles. During the aging treatment, the B2-NiAl intermetallic compound precipitated in the matrix and strengthened the matrix at 700°C.

After the high-temperature wear testing, a glazed layer and a heat-affected zone were formed, caused by the additional heat due to friction on the surface for both the HEAs. The dense glazed layer can decrease the friction coefficient and protect the substrate from oxidation.

TC02 alloy exhibited the lowest friction coefficient due to the dense glazed layer and an appropriate number of TiC particles in the matrix. The HEAs demonstrated exceptional oxidation

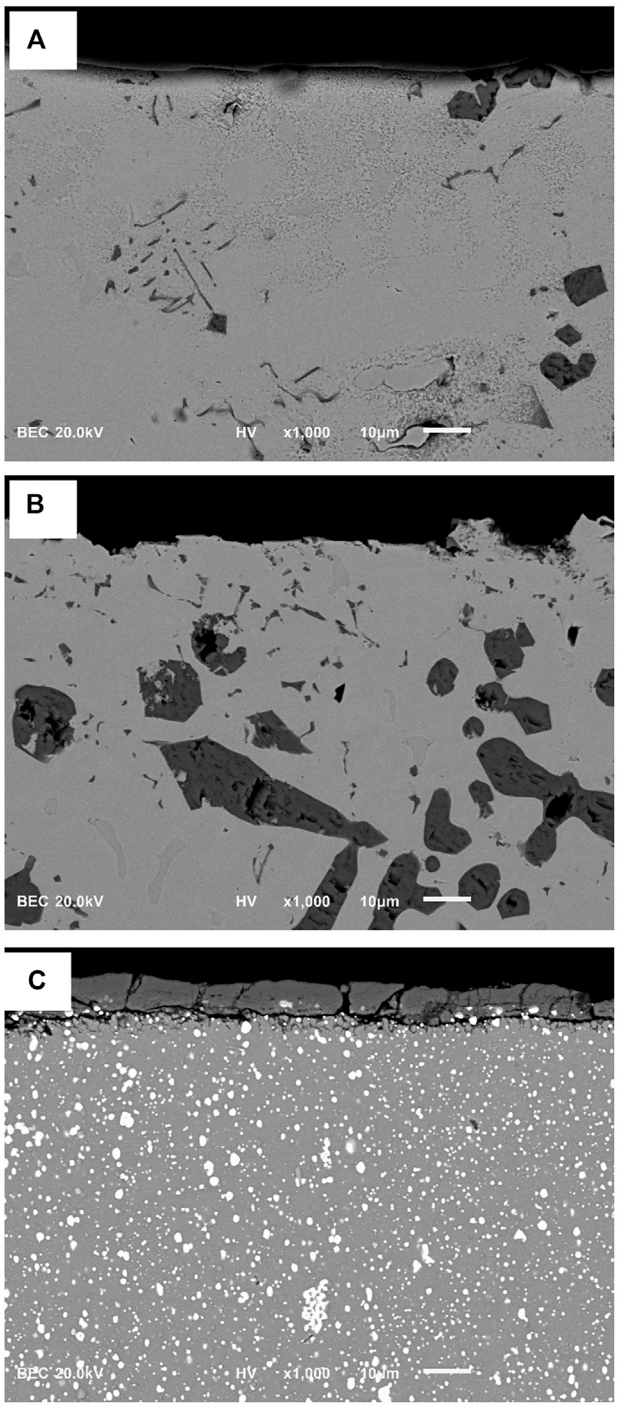


**FIGURE 10 |** Cross-sectional microstructure of the surface without worn at elevated temperature: **(A)** TC02 alloy, **(B)** TC05 alloy, and **(C)** M2 steel.

resistance and lower friction coefficient than M2 steel at elevated temperatures, which proves that HEAs have the potential for high-temperature applications.

## DATA AVAILABILITY STATEMENT

The original contributions presented in the study are included in the article/**Supplementary Material**, further inquiries can be directed to the corresponding author.

## AUTHOR CONTRIBUTIONS

C-HP, C-WT, and C-MK contributed to conception and design of the study. C-HP organized the database and performed the statistical analysis, and wrote the main draft of the article. S-MC wrote sections of the article. All authors contributed to article revision, read, and approved the submitted version.

## FUNDING

This work was financially supported by the "High Entropy Materials Center" from The Featured Areas Research Center Program within the framework of the Higher Education Sprout Project by the Ministry of Education (MOE) and from the Project MOST 109-2634-F-007-024 and 108-3017-F-007-002 by Ministry of Science and Technology (MOST) in Taiwan.

## SUPPLEMENTARY MATERIAL

The Supplementary Material for this article can be found online at: https://www.frontiersin.org/articles/10.3389/fmats.2021.787729/full#supplementary-material

## REFERENCES

Alvi, S., and Akhtar, F. (2019). High Temperature Tribology of CuMoTaWV High Entropy Alloy. *Wear* 426-427, 412–419. doi:10.1016/j.wear.2018.12.085

Aoh, J.-N., and Chen, J.-C. (2001). On the Wear Characteristics of Cobalt-Based Hardfacing Layer after thermal Fatigue and Oxidation. *Wear* 250, 611–620. doi:10.1016/s0043-1648(01)00668-8

Birol, Y. (2010). High Temperature Sliding Wear Behaviour of Inconel 617 and Stellite 6 Alloys. *Wear* 269, 664–671. doi:10.1016/j.wear.2010.07.005

Chen, S.-T., Tang, W.-Y., Kuo, Y.-F., Chen, S.-Y., Tsau, C.-H., Shun, T.-T., et al. (2010). Microstructure and Properties of Age-Hardenable AlxCrFe1.5MnNi0.5 Alloys. *Mater. Sci. Eng. A* 527, 5818–5825. doi:10.1016/j.msea.2010.05.052

Chen, M., Lan, L., Shi, X., Yang, H., Zhang, M., and Qiao, J. (2019). The Tribological Properties of Al0.6CoCrFeNi High-Entropy alloy with the σ

Phase Precipitation at Elevated Temperature. *J. Alloys Compd.* 777, 180–189. doi:10.1016/j.jallcom.2018.10.393

Cheng, J., Li, F., Zhu, S., Hao, J., Yang, J., Li, W., et al. (2017). High Temperature Tribological Properties of a nickel-alloy-based Solid-Lubricating Composite: Effect of Surface Tribo-Chemistry, Counterpart and Mechanical Properties. *Wear* 386-387, 39–48. doi:10.1016/j.wear.2017.06.001

Chuang, M.-H., Tsai, M.-H., Tsai, C.-W., Yang, N.-H., Chang, S.-Y., Yeh, J.-W., et al. (2013). Intrinsic Surface Hardening and Precipitation Kinetics of Al0.3CrFe1.5MnNi0.5 Multi-Component alloy. *J. Alloys Compd.* 551, 12–18. doi:10.1016/j.jallcom.2012.09.133

Deng, J., Liu, L., Yang, X., Liu, J., Sun, J., and Zhao, J. (2007). Self-lubrication of Al2O3/TiC/CaF2 Ceramic Composites in Sliding Wear Tests and in Machining Processes. *Mater. Des.* 28, 757–764. doi:10.1016/j.matdes.2005.12.003

Du, L. M., Lan, L. W., Zhu, S., Yang, H. J., Shi, X. H., Liaw, P. K., et al. (2019). Effects of Temperature on the Tribological Behavior of Al0.25CoCrFeNi High-Entropy alloy. *J. Mater. Sci. Technol.* 35, 917–925. doi:10.1016/j.jmst.2018.11.023

Fan, Q. C., Li, B. S., and Zhang, Y. (2014). The Microstructure and Properties of (FeCrNiCo)Al Cu High-Entropy Alloys and Their TiC-Reinforced Composites. *Mater. Sci. Eng. A* 598, 244–250. doi:10.1016/j.msea.2014.01.044

Fink, M. (1930). Wear Oxidation-A New Component of Wear. *Trans. Am. Soc. Steel Treat.* 18, 1026–1034.

Guo, S., Ng, C., Lu, J., and Liu, C. T. (2011). Effect of Valence Electron Concentration on Stability of Fcc or Bcc Phase in High Entropy Alloys. *J. Appl. Phys.* 109, 5. doi:10.1063/1.3587228

Hsu, C.-Y., Juan, C.-C., Wang, W.-R., Sheu, T.-S., Yeh, J.-W., and Chen, S.-K. (2011). On the superior Hot Hardness and Softening Resistance of AlCoCrxFeMo0.5Ni High-Entropy Alloys. *Mater. Sci. Eng. A.* 528, 3581–3588. doi:10.1016/j.msea.2011.01.072

Inman, I. A., and Datta, P. S. (2011). Studies of High Temperature Sliding Wear of Metallic Dissimilar Interfaces IV: Nimonic 80A versus Incoloy 800HT. *Tribol. Int.* 44, 1902–1919. doi:10.1016/j.triboint.2011.08.004

Inman, I. A., Datta, S., Du, H. L., Burnell-Gray, J. S., and Luo, Q. (2003). Microscopy of Glazed Layers Formed during High Temperature Sliding Wear at 750 °C. *Wear* 254, 461–467. doi:10.1016/s0043-1648(03)00134-0

Jiang, J., Stott, F. H., and Stack, M. M. (2004). A Generic Model for Dry Sliding Wear of Metals at Elevated Temperatures. *Wear* 256, 973–985. doi:10.1016/j.wear.2003.09.005

Jiang, X., Liu, W., Dong, S., and Xu, B. (2005). High Temperature Tribology Behaviors of brush Plated Ni-W-Co/SiC Composite Coating. *Surf. Coat. Technol.* 194, 10–15. doi:10.1016/j.surfcoat.2004.04.095

Joseph, J., Haghdadi, N., Shamlaye, K., Hodgson, P., Barnett, M., and Fabijanic, D. (2019). The Sliding Wear Behaviour of CoCrFeMnNi and AlxCoCrFeNi High Entropy Alloys at Elevated Temperatures. *Wear* 428-429, 32–44. doi:10.1016/j.wear.2019.03.002

Juan, C.-C., Tsai, M.-H., Tsai, C.-W., Lin, C.-M., Wang, W.-R., Yang, C.-C., et al. (2015). Enhanced Mechanical Properties of HfMoTaTiZr and HfMoNbTaTiZr Refractory High-Entropy Alloys. *Intermetallics* 62, 76–83. doi:10.1016/j.intermet.2015.03.013

Khajuria, G., and Wani, M. F. (2017). High-Temperature Friction and Wear Studies of Nimonic 80A and Nimonic 90 against Nimonic 75 under Dry Sliding Conditions. *Tribol Lett.* 65, 100. doi:10.1007/s11249-017-0881-1

Liu, H., Liu, J., Chen, P., and Yang, H. (2019). Microstructure and High Temperature Wear Behaviour of Iin-Ssitu TiC Reinforced AlCoCrFeNi-Based High-Entropy alloy Composite Coatings Fabricated by Laser Cladding. *Opt. Laser Technol.* 118, 140–150. doi:10.1016/j.optlastec.2019.05.006

Miracle, D. B., and Senkov, O. N. (2017). A Critical Review of High Entropy Alloys and Related Concepts. *Acta Mater.* 122, 448–511. doi:10.1016/j.actamat.2016.08.081

Pauschitz, A., Roy, M., and Franek, F. (2008). Mechanisms of Sliding Wear of Metals and Alloys at Elevated Temperatures. *Tribol. Int.* 41, 584–602. doi:10.1016/j.triboint.2007.10.003

Pei, Y. T., Galvan, D., De Hosson, J. T. M., and Cavaleiro, A. (2005). Nanostructured TiC/a-C Coatings for Low Friction and Wear Resistant Applications. *Surf. Coat. Technol.* 198, 44–50. doi:10.1016/j.surfcoat.2004.10.106

Prabhu, T. R., Arivarasu, M., Chodancar, Y., Arivazhagan, N., Sumanth, G., and Mishra, R. K. (2019). Tribological Behaviour of Graphite-Reinforced FeNiCrCuMo High-Entropy Alloy Self-Lubricating Composites for Aircraft Braking Energy Applications. *Tribology Lett.* 67, 15. doi:10.1007/s11249-019-1193-4

Stott, F. H., Lin, D. S., and Wood, G. C. (1973). The Structure and Mechanism of Formation of the 'glaze' Oxide Layers Produced on Nickel-Based Alloys during Wear at High Temperatures. *Corrosion Sci.* 13, 449–469. doi:10.1016/0010-938x(73)90030-9

Stott, F. H. (1998). The Role of Oxidation in the Wear of Alloys. *Tribology Int.* 31, 61–71. doi:10.1016/s0301-679x(98)00008-5

Takeuchi, A., and Inoue, A. (2005). Classification of Bulk Metallic Glasses by Atomic Size Difference, Heat of Mixing and Period of Constituent Elements and its Application to Characterization of the Main Alloying Element. *Mater. Trans.* 46, 2817–2829. doi:10.2320/matertrans.46.2817

Tsai, C.-W., Tsai, M.-H., Yeh, J.-W., and Yang, C.-C. (2010). Effect of Temperature on Mechanical Properties of Al0.5CoCrCuFeNi Wrought alloy. *J. Alloys Compd.* 490, 160–165. doi:10.1016/j.jallcom.2009.10.088

Tsai, M.-H., Yuan, H., Cheng, G., Xu, W., Jian, W. W., Chuang, M.-H., et al. (2013). Significant Hardening Due to the Formation of a Sigma Phase Matrix in a High Entropy alloy. *Intermetallics* 33, 81–86. doi:10.1016/j.intermet.2012.09.022

Tsao, L. C., Chen, C. S., and Chu, C. P. (2012). Age Hardening Reaction of the Al0.3CrFe1.5MnNi0.5 High Entropy alloy. *Mater. Des. (1980-2015)* 36, 854–858. doi:10.1016/j.matdes.2011.04.067

Yang, X., and Zhang, Y. (2012). Prediction of High-Entropy Stabilized Solid-Solution in Multi-Component Alloys. *Mater. Chem. Phys.* 132, 233–238. doi:10.1016/j.matchemphys.2011.11.021

Yeh, J.-W., Chen, S.-K., Lin, S.-J., Gan, J.-Y., Chin, T.-S., Shun, T.-T., et al. (2004). Nanostructured High-Entropy Alloys with Multiple Principal Elements: Novel alloy Design Concepts and Outcomes. *Adv. Eng. Mater.* 6, 299–303. doi:10.1002/adem.200300567

Yeh, J.-W. (2015). Physical Metallurgy of High-Entropy Alloys. *Jom* 67, 2254–2261. doi:10.1007/s11837-015-1583-5

**Conflict of Interest:** The authors declare that the research was conducted in the absence of any commercial or financial relationships that could be construed as a potential conflict of interest.

**Publisher's Note:** All claims expressed in this article are solely those of the authors and do not necessarily represent those of their affiliated organizations, or those of the publisher, the editors and the reviewers. Any product that may be evaluated in this article, or claim that may be made by its manufacturer, is not guaranteed or endorsed by the publisher.